NANO LETTERS

Letter

pubs.acs.org/NanoLett

Achromatic Metasurface Lens at Telecommunication Wavelengths

Mohammadreza Khorasaninejad,[†] Francesco Aieta,[†,‡] Pritpal Kanhaiya,[†,§] Mikhail A. Kats,[†,∥] Patrice Genevet,[†,⊥] David Rousso,[†,§] and Federico Capasso*[,†]

[†]School of Engineering and Applied Sciences, Harvard University, Cambridge, Massachusetts 02138, United States

[‡]Hewlett-Packard Laboratories, Palo Alto, California 94304, United States

[§]University of Waterloo, Waterloo, ON N2L 3G1, Canada

[∥]Department of Electrical and Computer Engineering, University of Wisconsin—Madison, Madison, Wisconsin 53706, United States

[⊥]Singapore Institute of Manufacturing Technology, 71 Nanyang Drive, Singapore 638075, Singapore

Supporting Information

ABSTRACT: Nanoscale optical resonators enable a new class of flat optical components called metasurfaces. This approach has been used to demonstrate functionalities such as focusing free of monochromatic aberrations (i.e., spherical and coma), anomalous reflection, and large circular dichroism. Recently, dielectric metasurfaces that compensate the phase dispersion responsible for chromatic aberrations have been demonstrated. Here, we utilize an aperiodic array of coupled dielectric nanoresonators to demonstrate a multiwavelength achromatic lens. The focal length remains unchanged for three wavelengths in the near-infrared region (1300, 1550, and 1800 nm). Experimental results are in agreement with full-wave simulations. Our findings are an essential step toward a realization of broadband flat optical elements.

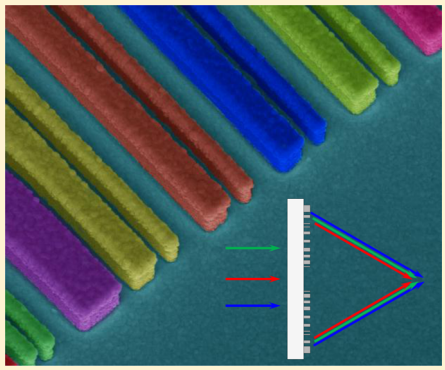

KEYWORDS: *Metasurfaces, dielectric resonators, achromatic, lens*

Lenses are one of the most commonly used components in any optical system with a wide range of applications from forming images of a scene to coupling in and out of optical fibers or integrated circuits.[1,2] Conventional refractive lenses rely on gradual phase accumulation via light propagation through a bulk material polished to a specific surface topology to shape the incident beam. This mechanism is in general strongly wavelength-dependent, resulting in chromatic aberrations. For example, changes in the focal length of most lenses for different wavelengths are expected, degrading their functionality in optical systems.[2,3]

Overcoming chromatic aberrations is required in various imaging systems ranging from conventional microscopy and photography to sophisticated astronomical spectroscopy[4] and optical coherence tomography.[3] Toward this end, double, triple, and quadruple lens combinations have been used to correct the chromatic aberrations yielding achromatic doublets, apochromatic lenses, and superachromatic objectives.[5−7] The achromatic, apochromatic, and superachromatic terms refer to paraxial color correction at two, three, and four wavelengths, respectively.[8,9] However, these multilens approaches are bulky and require complex designs and multiple materials.

Metasurfaces have their conceptual roots in early works on subwavelength gratings.[10−15] Using nanoresonators as phase shift elements, metasurfaces enable wavefront molding in a thin layer and have been used for demonstrations of beam bending,[16−18] lensing,[19−22] holography,[23−26] and polarization splitting.[27−31] The basic units of metasurfaces are subwavelength spaced nanoresonators whose responses (amplitude and phase) are wavelength-dependent. Although several works have reported that metasurfaces can be designed to operate over a broadband wavelength range,[16,17] the demonstrated devices all suffer from strong chromatic aberrations resulting from the intrinsic dispersive behavior of the resonators, thus compromising their performance. We note that even for resonators with small quality factors and corresponding broadband phase and amplitude responses, their operation still remains wavelength dependent. Recently, we demonstrated a metasurface design that overcomes this limitation, preserving its functionality for several wavelengths.[32] In the present work, we build upon those results and experimentally demonstrate an achromatic lens at the wavelengths of 1300, 1550, and 1800 nm. Our lens consists of an aperiodic arrangement of coupled rectangular dielectric resonators (RDRs) whose scattering phases are engineered to achieve dispersion-free focusing. One can conceptually visualize achromatic focusing in Figure 1a where three colors (red, green, and blue arbitrarily chosen for clarity) represent the three wavelengths of interest that are focused in the same line.

As light propagates from the metasurface interface to the focal plane, it accumulates a different amount of phase shift for

Received: May 1, 2015
Revised: July 2, 2015

DOI: 10.1021/acs.nanolett.5b01727
Nano Lett. XXXX, XXX, XXX−XXX

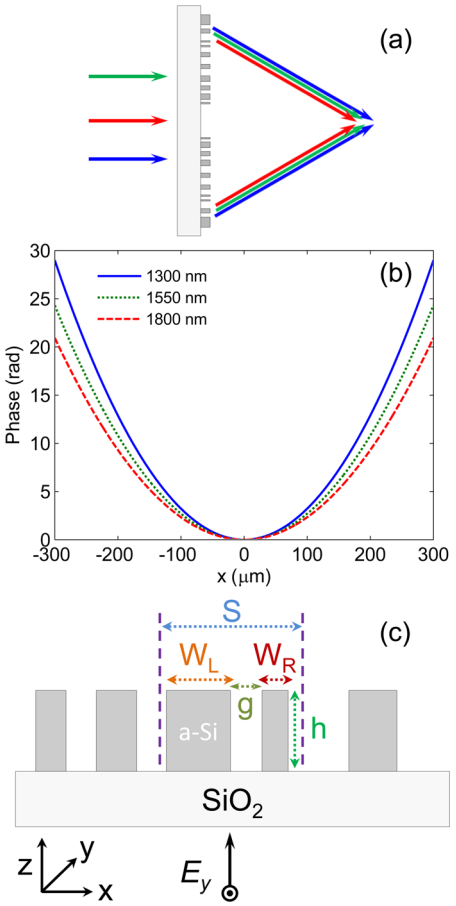

Figure 1. (a) Schematic of the metasurface lens. The metasurface is designed to function as a lens that focuses three different wavelengths into the same line. (b) Phase profiles of lens with numerical aperture NA = 0.04, diameter D = 600 μm, and focal length f = 7.5 mm for wavelengths of 1300, 1550, and 1800 nm as a function of the distance from the center of the lens. (c) Schematic of the metasurface consisting of amorphous silicon (a-Si) rectangular dielectric resonators (RDRs) on a fused silica substrate. Each unit cell (size S = 1 μm) contains two RDRs of widths W_L and W_R ($0 \leq W_L$ and $W_R \leq 600$ nm) and height h = 400 nm, separated by gap g ($0 \leq g \leq 800$ nm). The light is incident from the substrate and the polarization is along the length of RDRs (y-direction).

each wavelength. Therefore, to achieve equal focal lengths at different wavelengths, an achromatic metasurface must impart a wavelength dependent phase contribution to compensate for the dispersive accumulated phase. Figure 1b shows the necessary phase profiles for a lens with focal length f = 7.5 mm and diameter D = 600 μm for three different wavelengths (1300, 1550, 1800 nm). Several design degrees of freedom are needed to engineer a different phase profile for each wavelength. This is achieved using an array of coupled RDRs.[32] As shown in Figure 1c, each unit cell of the lens has size S and consists of two RDRs with widths W_L and W_R and gap g. The height of the RDRs is h = 400 nm. By varying the parameters W_L, W_R, and g, the resonances associated with different transverse electric and transverse magnetic modes can be adjusted to obtain the needed phase values of the scattered field (Figure 1b) for incident light polarized along the y-direction.

The fabrication process of the lens starts from a substrate of fused silica which is cleaned using acetone followed by oxygen ashing. Then, a 400 nm layer of amorphous silicon (a-Si) is deposited using plasma-enhanced chemical vapor deposition (PECVD). Double layer PMMA495/PMMA950 resists are successively spin-coated at a speed of 6000 rpm and baked on a hot plate at 180 °C for 5 min. Electron beam exposure is performed using an Elionix ELS-F125 system operating at 125 kV. Subsequently, the resist is developed in a mixture of methyl isobutyl ketone and isopropyl alcohol (MIBK:IPA 1:3) at room temperature for 60 s, rinsed in IPA for 30 s, and then blown dry in nitrogen. Next, aluminum (Al) is deposited by thermal evaporation as a mask of 20 nm thickness. Lift-off is carried out by soaking the sample in a solvent stripper (Remover PG from Microchem). Inductively coupled plasma-reactive ion etching (ICP-RIE) is then performed to define the RDRs. A mixture of SF_6 and CF_4 is used, resulting in a highly anisotropic etching of the a-Si.[33] Finally the Al is removed. Optical and scanning electron micrograph images of the fabricated lens are shown in Figure 2a–b.

We performed the optical characterization of the fabricated lens using the setup illustrated in Figure 2c. A supercontinuum laser (NKT "SuperK") equipped with a tunable bandpass filter (line-width of 15 nm) is used as a source. The laser beam is collimated by a broadband reflective collimator and passed through a linear polarizer (electric field along y-direction) and then through the sample (metasurface lens). The light transmitted by the sample is collected by a microscope objective lens paired with a tube lens to form an image on an InGaAs camera. The objective lens, tube lens, and camera are all mounted on an optical breadboard to keep their relative distances fixed. The breadboard is placed on a xyz-stage and is translated along the optical axis to record an image (intensity distribution) of the propagating light after interaction with the metasurface lens. Results of these measurements are shown in Figure 3a–c and are in agreement with the simulations in Figure 3d–f. The latter are obtained by performing full wave analysis of the lens using the finite-difference time-domain (FDTD) method (Lumerical FDTD Solutions). For simulations, we used the same refractive index for a-Si as reported in ref 32. For a better quantitative comparison, the intensity distributions across the focal plane of the lens (z = ~7.5 mm) are measured for desired wavelengths and shown in Figure 4. Two dimensional focal plane images captured by the camera at the three design wavelengths are shown in Figure S1 of Supporting Information (SI). These results confirm that the lens indeed focuses the incident light at the same focal length for wavelengths of 1300, 1550, and 1800 nm. Full-width at half maximums (FWHMs) of 27.5, 29, and 25 μm are measured for the wavelengths of 1300, 1550, and 1800 nm, respectively, which are close to the diffraction limit (17, 20, and 23 μm, for a lens with numerical aperture NA = 0.04). Absolute efficiencies of 15%, 10%, and 21% are measured for wavelengths of 1300, 1550, and 1800 nm, respectively, and are less than the values predicted by simulations (24%, 22%, and 28%). Absolute efficiency is defined as the amount of power in the beam waist at the focal line, divided by the input power. The beam waist is the full width of the normalized intensity at $1/e^2$ and is calculated by fitting the measured intensity distribution at the focal line to a Gaussian function. The input power is the amount of collimated power (beam diameter of 4 mm) that passes through an aperture with the same dimensions as the lens (600 μm × 600 μm). The difference between measured and simulated efficiency values arises mainly from the imperfect phase realization (see Figure S2 of SI) and nonuniform RDR

DOI: 10.1021/acs.nanolett.5b01727
Nano Lett. XXXX, XXX, XXX–XXX

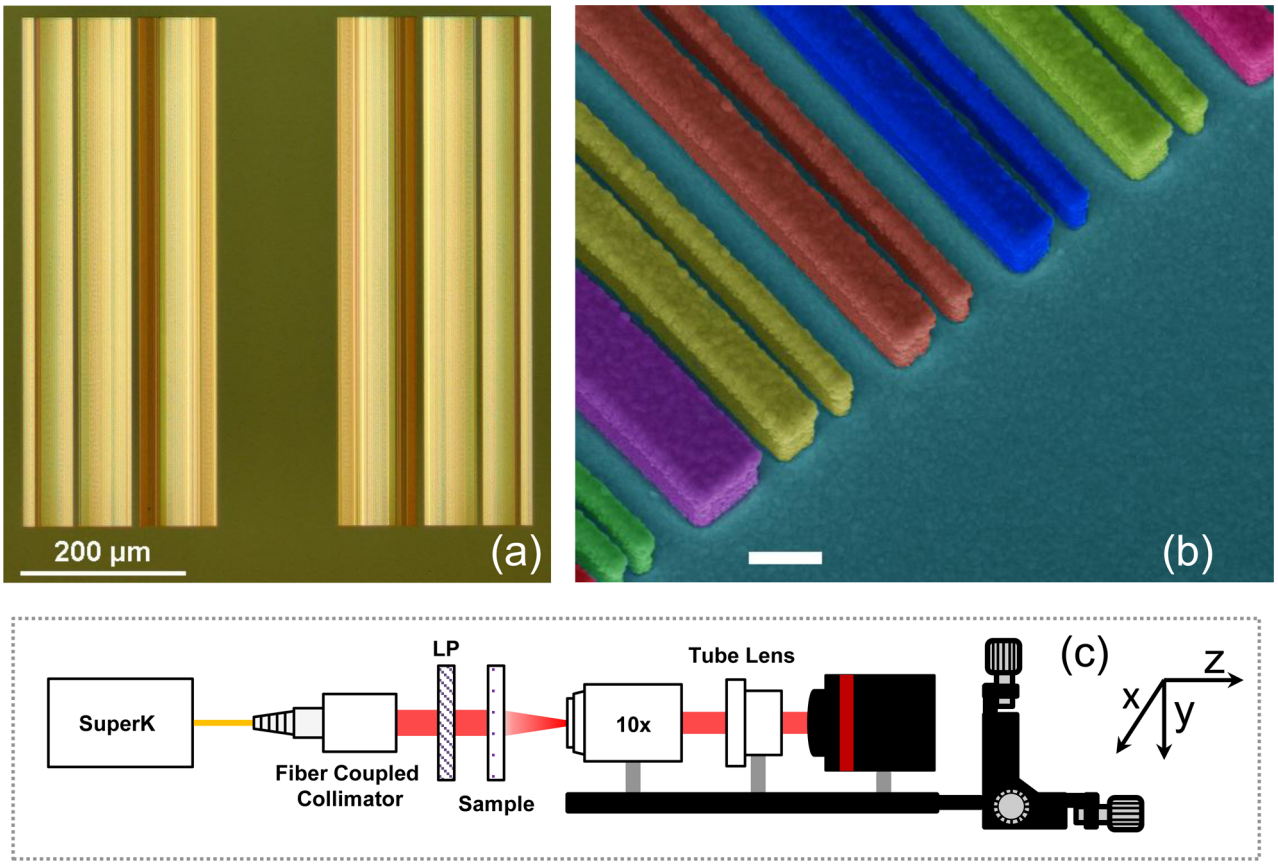

Figure 2. (a) Top-view optical image of the metasurface lens. (b) False colored side-view scanning electron micrograph (SEM) image of the metasurface lens. Each unit cell is identified by a different color. Scale bar is 400 nm. Gold (30 nm) is sputtered on the lens to facilitate SEM imaging. (c) The light source is a supercontinuum laser (SuperK) with a tunable band-pass filter and a fiber coupled output. The output beam is collimated and linearly polarized (LP). The objective (10×) and tube lenses form an image of the beam after the metasurface lens onto the InGaAs camera.

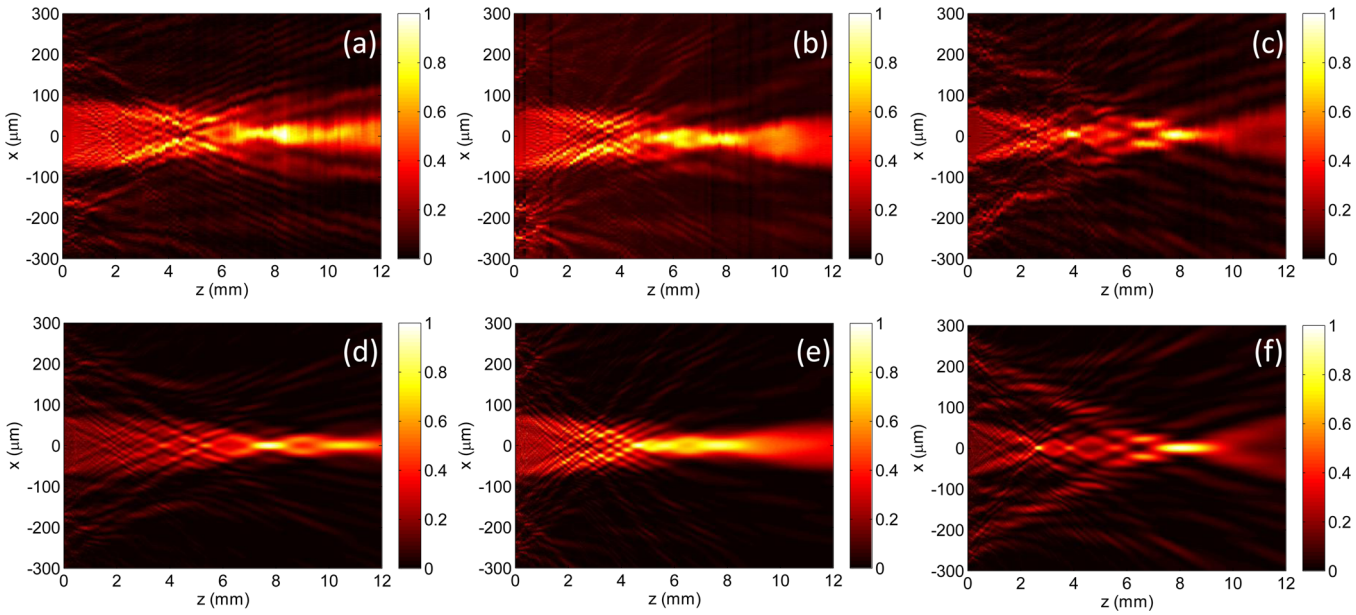

Figure 3. Measured intensities in the $x-z$ plane after the lens at wavelengths (a) 1300 nm, (b) 1550 nm, and (c) 1800 nm and the corresponding FDTD simulations (d–f). Measurements are performed using the setup shown in Figure 2c. First, the objective lens is focused on the lens to capture the first image. The objective lens, tube lens, and InGaAs camera are then moved ∼120 μm away from the lens along the optical axis, z-direction, to capture the second image. This process is repeated to capture the remaining images up to at a distance z = 12 mm from the metasurface. The intensity distributions of each captured image, along the $x-z$ plane, are stitched together forming an $x-z$ plane intensity profile. For all simulations and experiments, polarization is along the y-direction.

DOI: 10.1021/acs.nanolett.5b01727
Nano Lett. XXXX, XXX, XXX−XXX

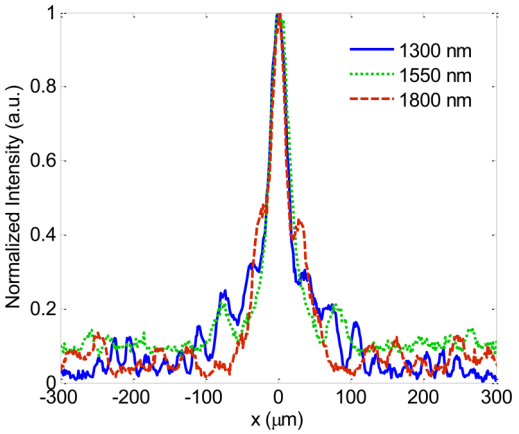

Figure 4. Measured intensity profiles across the focal plane of the lens for three wavelengths of 1300, 1550, and 1800 nm. Intensity profiles are extracted from Figure 3a–c along the *x*-direction and at the focal length.

scattering amplitudes across the metasurface. The latter can be improved by choice of more advanced design strategies such as genetic algorithms for optimizing the resonators geometry. Computationally efficient methods will be also important for designing metasurface lenses with large numerical apertures. In addition, we note that the theoretical transmissions are 48%, 48%, and 65% for wavelengths of 1300, 1550, and 1800 nm, respectively. Therefore, reducing the reflection by either a metasurface stack[21,34] or tuning the spectral position of electric and magnetic dipole resonances of RDRs to achieve impedance matching[35] condition can also improve the performance.

We characterized the lens at several different wavelengths and measured the focal length as shown in Figure 5. As

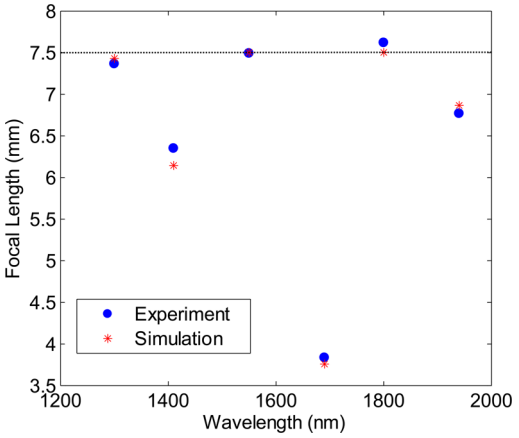

Figure 5. Measured and simulated focal lengths of the metasurface lens for several wavelengths. The focal length is fixed at 7.5 mm for the design wavelengths (1300, 1550, and 1800 nm) whereas for wavelengths of 1410, 1690, and 1940 nm where no phase compensation was performed, the focal length deviates from this value.

expected for the wavelengths of 1410, 1690, and 1940 nm where phase compensation was not performed, the focal lengths changed as a result of chromatic aberrations. For instance, the focal length shifted to z = 3.83 mm at wavelength λ = 1690 nm. Measured and simulated intensities in the x–z plane at this wavelength are shown in Figure S3 of SI. We also studied the effect of incidence angle on the performance of the lens. For these measurements, first, the objective lens is fixed at the focal length of the lens to capture the light distribution. Then we changed the incidence angle relative to the normal to the surface of the lens (in x–z plane) and captured the image and calculated the fwhm at each angle and same location. Results of these measurements are shown in Figure 6 where

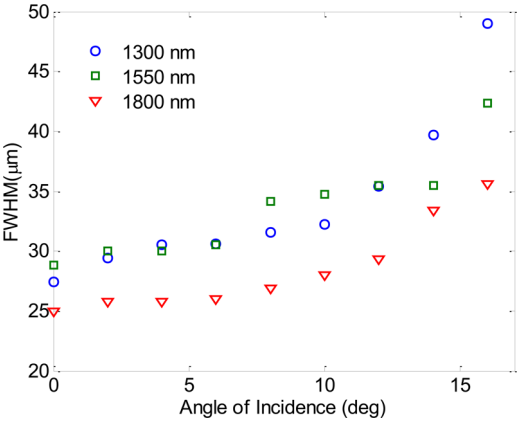

Figure 6. Measured full-width at half-maximum of the lens at the focal line (z = 7.5 mm) versus angle of incidence and wavelengths of 1300, 1550, and 1800 nm. Incidence angle is changed in the x–z plane.

there is minimal change in fwhm for angles of incidence up to ~10°. In addition, the simulated focal lengths of the lens at three design wavelengths versus incidence angle are shown in Figure S4 of SI.

In summary, we experimentally demonstrated an achromatic metasurface lens operating at three wavelengths in the near-infrared. This approach can be adapted to achieve wavelength independent optical components in a compact configuration, overcoming a fundamental limitation of existing optical components. Our demonstration is a significant step toward the realization of broadband optical elements that have applications ranging from optical microscopy to integrated optics and astronomical imaging. Achromatic flat optics could also provide innovative solutions for applications in imaging and lightweight vision.

■ ASSOCIATED CONTENT

Ⓢ Supporting Information

The design details and supplementary figures. The Supporting Information is available free of charge on the ACS Publications website at DOI: 10.1021/acs.nanolett.5b01727.

■ AUTHOR INFORMATION

Corresponding Author

*E-mail: capasso@seas.harvard.edu. Phone: 617 384 7611. Fax: 617 495 2875.

Notes

The authors declare no competing financial interest.

■ ACKNOWLEDGMENTS

This work was supported in part by the Air Force Office of Scientific Research (MURI: FA9550-14-1-0389). Support from Google Inc. is gratefully acknowledged. We thank E. Hu for the supercontinuum laser (NKT "SuperK"). Fabrication work was carried out in the Harvard Center for Nanoscale Systems, which is supported by the NSF.

DOI: 10.1021/acs.nanolett.5b01727
Nano Lett. XXXX, XXX, XXX–XXX

REFERENCES

(1) Pollock, C. R.; Lipson, M. *Integrated photonics*; Kluwer Academic: Boston, 2003.
(2) Gu, M. *Advanced optical imaging theory*; Springer Science and Business Media: New York, 1993.
(3) Hartl, J.; Li, X. D.; Chudoba, C.; Ghanta, R. K.; Ko, T. H.; Fujimoto, J. G.; Ranka, J. K.; Windeler, R. S. *Opt. Lett.* **2001**, *26*, 608−610.
(4) Ren, D.; Allington Smith, J. R. *Opt. Eng.* **1999**, *38*, 537−542.
(5) Robb, P. N.; Mercado, R. I. *J. Opt. Soc. Am.* **1983**, *73*, 1882.
(6) Buchdahl, H. A. *Appl. Opt.* **1985**, *24*, 1878.
(7) Herzberger, M.; Salzberg, C. D. *J. Opt. Soc. Am.* **1962**, *52*, 420.
(8) Pedrotti, F. L.; Pedrotti, L. S. *Introduction to Optics*; Prentice-Hall: Upper Saddle River, NJ, 1987.
(9) Mercado, R.; Ryzhikov, L. *Proc. SPIE* **1998**, *3482*, 321−331.
(10) Stork, W.; Streibl, N.; Haidner, H.; Kipfer, P. *Opt. Lett.* **1991**, *16*, 1921−1923.
(11) Farn, W. M. *Appl. Opt.* **1992**, *31*, 4453−4458.
(12) Haidner, H.; Kipfer, P.; Sheridan, J. T.; Schwider, J.; Streibl, N.; Collischon, M.; Hutfless, J.; März, M. *Infrared Phys.* **1993**, *34*, 467−475.
(13) Chen, F. T.; Craighead, H. G. *Opt. Lett.* **1995**, *20*, 121−123.
(14) Astilean, S.; Lalanne, P.; Chavel, P.; Cambril, E.; Launois, H. *Opt. Lett.* **1998**, *23*, 552−554.
(15) Ribot, C.; Lee, M. S. L.; Collin, S.; Bansropun, S.; Plouhinec, P.; Thenot, D.; Cassette, S.; Loiseaux, B.; Lalanne, P. *Adv. Opt. Mater.* **2013**, *1*, 489−493.
(16) Yu, N.; Genevet, P.; Kats, M. A.; Aieta, F.; Tetienne, J. P.; Capasso, F.; Gaburro, Z. *Science* **2012**, *334*, 333.
(17) Ni, X.; Emani, N. K.; Kildishev, A. V.; Boltasseva, A.; Shalaev, V. M. *Science* **2012**, *335*, 427.
(18) Pinchuk, A. O.; Schatz, G. C. *J. Opt. Soc. Am. A* **2007**, *24*, 39−44.
(19) West, P. R.; Stewart, J. L.; Kildishev, A. V.; Shalaev, V. M.; Shkunov, V. V.; Strohkendl, F.; Zakharenkov, Y. A.; Dodds, R. K.; Byren, R. *Opt. Express* **2014**, *22*, 26212−26221.
(20) Aieta, F.; Genevet, P.; Kats, M. A.; Yu, N.; Blanchard, R.; Gaburro, Z.; Capasso, F. *Nano Lett.* **2012**, *12*, 4932−4936.
(21) Monticone, F.; Estakhri, N. M.; Alù, A. *Phys. Rev. Lett.* **2013**, *110*, 203903.
(22) Fattal, D.; Li, J.; Peng, Z.; Fiorentino, M.; Beausoleil, R. G. *Nat. Photonics* **2010**, *4*, 466−470.
(23) Genevet, P.; Capasso, F. *Rep. Prog. Phys.* **2015**, *78*, 024401.
(24) Larouche, S.; Tsai, Y. J.; Tyler, T.; Jokerst, N. M.; Smith, D. R. *Nat. Mater.* **2012**, *11*, 450−454.
(25) Zheng, G.; Mühlenbernd, H.; Kenney, M.; Li, G.; Zentgraf, T.; Zhang, S. *Nat. Nanotechnol.* **2015**, *10*, 308−312.
(26) Chen, W. T.; Yang, K. Y.; Wang, C. M.; Huang, Y. W.; Sun, G.; Chiang, I. D.; Liao, C. Y.; Hsu, W. L.; Lin, H. T.; Tsai, D. P. *Nano Lett.* **2014**, *14*, 225−230.
(27) Yu, N.; Aieta, F.; Genevet, P.; Kats, M.; Gaburro, Z.; Capasso, F. *Nano Lett.* **2012**, *12*, 6328−6333.
(28) Khorasaninejad, M.; Crozier, K. B. *Nat. Commun.* **2014**, *5*, 5386.
(29) Khorasaninejad, M.; Zhu, W.; Crozier, K. B. *Optica* **2015**, *2*, 376−382.
(30) Sun, S.; Yang, K.-Y.; Wang, C.-M.; Juan, T.-K.; Chen, W. T.; Liao, C. Y.; He, Q.; Xiao, S.; Kung, W.-T.; Guo, G.-Y.; Zhou, L.; Tsai, D. P. *Nano Lett.* **2012**, *12*, 6223−6229.
(31) Lin, J.; Mueller, J. P. B.; Wang, Q.; Yuan, G.; Antoniou, N.; Yuan, X.-C.; Capasso, F. *Science* **2013**, *340*, 331−334.
(32) Aieta, F.; Kats, M. A.; Genevet, P.; Capasso, F. *Science* **2015**, *347*, 1342.
(33) Khorasaninejad, M.; Abedzadeh, N.; Walia, J.; Patchett, S.; Saini, S. S. *Nano Lett.* **2012**, *12*, 4228−4234.
(34) Pfeiffer, C.; Grbic, A. *Phys. Rev. Lett.* **2013**, *110*, 197401.
(35) Krasnok, A. E.; Miroshnichenko, A. E.; Belov, P. A.; Kivshar, Y. S. *Opt. Express* **2012**, *20*, 20599−20604.

DOI: 10.1021/acs.nanolett.5b01727
Nano Lett. XXXX, XXX, XXX−XXX